Determination of the lattice susceptibility within the dual fermion method

Gang Li, Hunpyo Lee, and Hartmut Monien
Bethe Center for Theoretical Physics, Universität Bonn, 53115 Bonn, Germany
(Received 15 August 2008; published 7 November 2008)

In this paper, we present the details of the dual fermion (DF) method to study the nonlocal corrections to the single-site dynamical mean-field theory (DMFT). The DMFT two-particle Green's function is calculated using continuous-time quantum Monte Carlo method. The momentum dependence of the vertex function is analyzed and its renormalization based on the Bethe-Salpeter equation is performed in the particle-hole channel. We found magnetic instability for both the dual and the lattice fermions. Furthermore, the lattice fermion susceptibility is calculated in this method and also in another recently proposed method, namely, dynamical vertex approximation (DΓA). The comparisons between these two methods are presented in both weak- and strong-coupling regions. Compared to the results from the quantum Monte Carlo calculation, the susceptibility obtained from the DF and DΓA methods are satisfactory.

DOI: 10.1103/PhysRevB.78.195105 PACS number(s): 71.10.Fd, 71.28.+d, 71.45.Gm

I. INTRODUCTION

Strongly correlated electron systems, such as the heavy fermion compounds and high-temperature superconductors, have gained much attention from both theoretical and experimental points of view. The competition between the kinetic energy and fermion Coulomb interaction generates a lot of fascinating phenomena. Many theoretical approaches have been developed to understand the nature of the strongly correlated materials. The widely used perturbative methods, such as random-phase approximation (RPA), fluctuation exchange (FLEX),[1,2] and the two-particle self-consistent (TPSC) (Refs. 3 and 4) method are based on the expansion in the Coulomb interaction which are only valid for the weak-coupling system. To go beyond the perturbative approximation and to gain insight of the correlation effects in the fermion systems, new theoretical methods are needed. Dynamical mean-field theory (DMFT) (Refs. 5–7) is a big step forward in the understanding of metal-insulator transition.

Dynamical mean-field theory maps a many-body interacting system on a lattice onto a single impurity embedded in a noninteracting bath. Such mapping becomes exact in the limit of infinite coordination number. All local and temporal fluctuations are taken into account in this theory, and spatial fluctuations are treated on the mean-field level. DMFT has been proven a successful theory in describing the basic physics of the Mott-Hubbard transition. But the nonlocal correlation effect cannot always be omitted. Although, the straightforward extensions of DMFT (Refs. 8–12) have captured the influence of short-range correlations, these methods are not capable of describing the collective behavior, e.g., spin-wave excitations of many-body system. At the same time, most of the numerically exact impurity solvers require a substantial amount of time to achieve a desired accuracy even on a small cluster, which makes the investigation of larger lattice hard.

Recently, some efforts have been made to take the spatial fluctuations into account in different ways.[13–17] These methods construct the nonlocal contributions to DMFT from the local two-particle vertex. Self-energy function contains only certain diagrams, which makes them only approximately include the nonlocal corrections. Various cluster DMFT methods try to exactly incorporate the nonlocality within a small reference system and treat the remaining correlations as mean field. In contrast to cluster DMFT methods, the long-range information is naturally included in these new methods from their construction. Our calculations showed that in the dual fermion method and the dynamical vertex approximation[13,14] such approximate momentum-dependent self-energy and vertex function are normally sufficient to generate reliable results compared to the numerically exact calculations.

In this paper we apply the dual fermion (DF) method proposed by Rubtsov *et al.*[14] to consider the vertex renormalization through the Bethe-Salpeter equation. We mainly focus on the lattice susceptibility calculation. We will show that even with the simplest approximation of the DF self-energy, the lattice susceptibility calculated from this method nicely repeats the computationally expensive QMC results. We will also extend another similar method proposed by Toschi *et al.*[13] to investigate the two-particle properties. The discussion of relation and difference between these two methods will also be presented.

The paper is organized as follows. In Sec. II we summarize the basic idea of the DF method and present the details of our calculation. The DMFT two-particle Green's function and the corresponding vertex calculation are implemented in continuous-time quantum Monte Carlo (CT-QMC) in Sec. III. The frequency dependent vertex is modified through the Bethe-Salpeter equation to obtain the momentum dependence in Sec. IV. In Sec. V we present the calculation of the lattice susceptibility and compare it to QMC results. In Sec. VI we extend the works of Toschi *et al.*[13] to calculate the lattice susceptibility and compare it to those from the DF calculation. The conclusions are summarized in Sec. VII.

II. DF METHOD

We study the general one-band Hubbard model at two dimension

$$H = \sum_{k,\sigma} \epsilon_{k,\sigma} c^{\dagger}_{k\sigma} c_{k\sigma} + U \sum_{i} n_{i\uparrow} n_{i\downarrow}, \tag{1}$$

where $c^{\dagger}_{k\sigma}(c_{k\sigma})$ creates (annihilates) an electron with spin σ and momentum k. The dispersion relation is $\epsilon_k = -2t(\cos k_x + \cos k_y)$. The basic idea of the DF method[14] is to transform the hopping between different sites into the coupling to an auxiliary field $f(f^{\dagger})$. By doing so, each lattice site can be viewed as an impurity. The interacting lattice problem is reduced to solving a multi-impurity problem which couples to the auxiliary field. The impurity problem can be solved using the standard DMFT calculation. After integrating out the lattice fermions degrees of freedom $c(c^{\dagger})$ one can obtain an effective theory of the auxiliary variables, where DMFT two-particle vertex function serves as the effective interaction. An exact relation between the lattice Green's function and the DF Green's function allows us to determine the lattice fermion Green's function from the latter.

To explicitly demonstrate the above idea we start from the lattice action which can be written as

$$S[\bar{c}, c] = \sum_{i} S^{i}_{\mathrm{imp}} - \sum_{k,\sigma} (\Delta_\nu - \epsilon_k) \bar{c}_{k\sigma} c_{k\sigma}, \tag{2}$$

where S^{i}_{imp} is the action of an impurity coupling to a dynamical bath described by Δ_ν. Applying the Gaussian identity to the bilinear term, we decouple the lattice sites to a collection of impurities which couple to an auxiliary field $f(f^{\dagger})$:

$$S[\bar{c}, c; \bar{f}, f] = \sum_{i} S^{i}_{\mathrm{imp}} + \sum_{k,\sigma} [g_\nu^{-1} (\bar{c}_{k\sigma} f_{k\sigma} + \mathrm{H.c.}) + g_\nu^{-2} (\Delta_\nu - \epsilon_k)^{-1} \bar{f}_{k\sigma} f_{k\sigma}]. \tag{3}$$

The equivalence of Eqs. (2) and (3) form an exact relation between the Green's function of the lattice electrons and the DF

$$G_k = g_\nu^{-2} (\Delta_\nu - \epsilon_k)^{-2} G^{d}_{k} + (\Delta_\nu - \epsilon_k)^{-1}. \tag{4}$$

This relation is easily derived by taking the derivative of the two actions over ϵ_k. Equation (4) allows us to solve the many-body lattice problem basing on the single-site DMFT, which is different from the straightforward cluster extensions. The problem now is how to solve the DF Green's function G^{d}_{k}. It is determined by integrating Eq. (3) over $\bar{c}$ and c, which yields a Taylor expansion series in power of $\bar{f}$ and f. The Grassmann integral ensures that $\bar{f}$ and f appear only in pairs associated with the lattice fermion n-particle vertex obtained from the single-site DMFT calculation. Up to now, there is no any approximation involved in the construction of the DF method. Basically, the perturbation expansion of the dual variables (auxiliary field) f contains all possible combinations of the DF Green's function and its many-particle vertices. In this paper we restrict our considerations to the two-particle vertex $\gamma^{(4)}$. Then the effective action of the dual variables has the form

$$S[\bar{f}, f] = -\sum_{k,\sigma} \bar{f}_{k,\sigma} [G^{d}_{0}(k)]^{-1} f_{k,\sigma} + \sum_{i} V(\bar{f}, f). \tag{5}$$

The bare DF Green's function $G^{d}_{0}(k)$ is given as

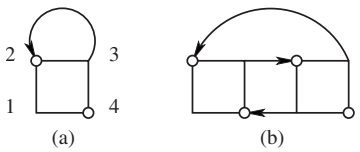

FIG. 1. The first two order DF self-energy diagrams. They are composed of the local two-particle vertex function and the DF propagator.

$$G^{d}_{0}(k) = -g^{2}_{\nu} / [(\Delta_\nu - \epsilon_k)^{-1} + g_\nu]. \tag{6}$$

The effective interaction $V(\bar{f}, f)$ of the DF is

$$V(\bar{f}, f) = -\frac{1}{4} \bar{f}_{\sigma_1} \bar{f}_{\sigma_2} \gamma^{(4)}_{\sigma_{1234}} f_{\sigma_3} f_{\sigma_4}. \tag{7}$$

Expanding the effective action (5) in $\gamma^{(4)}$ yields a Taylor series which represents all possible combinations of the DF Green's function and $\gamma^{(4)}$. The second approximation of the DF method is that only the first two order expansion terms are taken into account. Higher order diagrams are expected to be not important. Generally, this is not always true since such weak-coupling expansion is not appropriate in the strong-coupling region. But our calculation shows that the first two order diagrams of the DF self-energy are the main contributions of the nonlocal contribution to the single-site DMFT.

These two diagrams are shown in Fig. 1. Diagram (a) vanishes for the bare DF Green's function since this diagram exactly corresponds to the DMFT self-consistency condition. Therefore the first nonlocal contribution is given by diagram (b). The self-energies for these two diagrams are

$$\Sigma^{(1)}_{\sigma}(k_1) = \frac{T}{N} \sum_{\sigma', k_2} G^{d}_{\sigma'}(k_2) \gamma^{(4)}_{\sigma\sigma'}(\nu, \nu'; \nu', \nu), \tag{8a}$$

$$\Sigma^{(2)}_{\sigma}(k_1) = -\frac{T^2}{2N^2} \sum_{2,3,4} G^{d}_{\sigma_2}(k_2) G^{d}_{\sigma_3}(k_3) G^{d}_{\sigma_4}(k_4) \gamma^{(4)}_{\sigma_{1234}} \times (\nu_1, \nu_2; \nu_3, \nu_4) \gamma^{(4)}_{\sigma_{4321}} \times (\nu_4, \nu_3; \nu_2, \nu_1) \delta_{k_1+k_2, k_3+k_4} \delta_{\sigma_1+\sigma_2, \sigma_3+\sigma_4}. \tag{8b}$$

Here space-time notation is used $k = (\mathbf{k}, \nu)$, $q = (\mathbf{q}, \omega)$. Fermionic Matsubara frequency is $\nu_n = (2n+1)\pi/\beta$ and bosonic frequency is $\omega_m = 2m\pi/\beta$, where β is the inverse temperature. The full DF Green's function is obtained from the Dyson equation

$$[G^{d}(k)]^{-1} = [G^{d}_{0}(k)]^{-1} - \Sigma^{d}(k). \tag{9}$$

The algorithm of the whole calculation is:

(1) Set initial value of Δ_ν for the first DMFT loop.

(2) Determine the converged single-site DMFT Green's function g_ν from the hybridization function Δ_ν. The self-consistency condition ensures that the first diagram of the DF self-energy is zero.

(3) Go through the DMFT loop once again to calculate the two-particle Green's function and the corresponding γ function. The method for determining the γ function is imple-

mented for both strong- and weak-coupling CT-QMC in the next section of this paper.

(4) Start an inner loop calculation to determine the DF Green's function and in the end the lattice Green's function.

(a) From Eqs. (8a) and (8b) to calculate the DF self-energy.

(b) The full DF Green's function is given from the Dyson Eq. (9).

(c) Iteratively solve Eqs. (8a), (8b), and (9) until the convergence of the DF Green's function is achieved.

(d) The lattice Green's function is then given by Eq. (4) from that of the DF.

(5) Fourier transform the momentum lattice Green's function into real space and determine a new hybridization function Δ_ν from the on-site lattice Green's function G_{ii}.

(6) Go back to the step (3) and iteratively perform the outer loop until the hybridization Δ_ν does not change any more.

Although diagram (a) is exactly zero for the bare DF Green's function, it gives nonzero contribution to the DF self-energy from the second loop where the DF Green's function is updated from Eq. (9). As a result, the hybridization function should also be updated before the execution of the next DMFT loop. This is simply done by setting the local full DF Green's function to zero, together with the condition that the old hybridization function forces the bare local DF Green's function to be zero ($\Sigma_k G^{0,d}_{\nu,k}=0$). We obtain a set of equations

$$\frac{1}{N}\sum_k [G_{\nu,k}-(\Delta_\nu^{\text{new}}-\epsilon_k)^{-1}]g_\nu^2(\Delta_\nu^{\text{new}}-\epsilon_k)^2=0, \quad (10a)$$

$$\frac{1}{N}\sum_k [G^0_{\nu,k}-(\Delta_\nu^{\text{old}}-\epsilon_k)^{-1}]g_\nu^2(\Delta_\nu^{\text{old}}-\epsilon_k)^2=0, \quad (10b)$$

which yields

$$\Delta_\nu^{\text{new}}-\Delta_\nu^{\text{old}}\approx\frac{1}{N}\sum_k (G_{\nu,k}-G^0_{\nu,k})(\Delta_\nu^{\text{old}}-\epsilon_k)^2. \quad (11)$$

This equation finally gives us the relation between the new and old hybridization functions

$$\Delta_\nu^{\text{new}}=\Delta_\nu^{\text{old}}+g_\nu^2 G^d_{\text{loc}}. \quad (12)$$

In the whole calculation, the DF perturbation calculation converges quickly. The most time consuming part is the determination of the two-particle Green's function in DMFT. The two-particle Green's function $\chi_{\sigma,\sigma'}$ is a fully antisymmetric function.[18,19] One does not need to calculate $\chi_{\sigma,\sigma'}$ for all the frequency points within the cutoff in Matsubara space, only on a few special points $\chi_{\sigma,\sigma'}$ needs to be measured and the values for the other frequency points are then given from the solutions of those special points through the antisymmetric property. Another acceleration is for the momentum sum which always has a convolution type in our calculation; it can be easily calculated by fast Fourier transform (FFT).

III. CT-QMC AND TWO-PARTICLE VERTEX

From the above analysis, we know that the key idea of the DF method is to construct the nonlocal contribution from the auxiliary field and the DMFT two-particle Green's function. Therefore it is quite important to accurately determine the two-particle vertex. Here we adapt the newly developed CT-QMC method[20–22] to calculate the two-particle Green's function χ.

First we briefly outline the CT-QMC technique. For more details, we refer the readers to Refs. 20–22. Here we focus on the measurement of the two-particle Green's function. Two variants of the CT-QMC methods have been proposed based on the diagrammatic expansion. Unlike the Hirsch-Fye method, these methods do not have Trotter error and can approach the low-temperature region relatively easily. In the weak-coupling method[20] the noninteracting part of the partition function is kept unchanged and the interaction term is expanded as Taylor series. Wick's theorem ensures that the corresponding expansion can be written as a determinant at each order

$$\mathcal{Z}=\sum_k \frac{(-U)^k}{k!}\int d\tau_1\ldots d\tau_k \det[D_\uparrow D_\downarrow], \quad (13)$$

with

$$D_\uparrow D_\downarrow=\begin{pmatrix}\cdots & \mathcal{G}_\uparrow(\tau_1-\tau_k)\\ \cdots & \cdots\end{pmatrix}\begin{pmatrix}\cdots & \cdots\\ \mathcal{G}_\downarrow(\tau_k-\tau_1) & \cdots\end{pmatrix}, \quad (14)$$

where S_0 is the noninteracting action, $\mathcal{G}$ is the inverse Weiss field, and the one-particle Green's function is measured as

$$G(\nu)=\mathcal{G}(\nu)-\frac{1}{\beta}\mathcal{G}(\nu)\sum_{i,j} M_{i,j}e^{i\nu(\tau_i-\tau_j)}\mathcal{G}(\nu). \quad (15)$$

In the strong-coupling method the effective action is expanded in the hybridization function by integrating out the noninteracting bath degrees of freedom. Such an expansion also yields a determinant

$$\mathcal{Z}=\mathcal{Z}_{\text{loc}}\sum_{k_\sigma}\frac{1}{k_\sigma!}\int d\tau_1^s\ldots d\tau_{k_\sigma}^s\int d\tau_1^e\ldots d\tau_{k_\sigma}^e\langle T_\tau\prod_\sigma c_\sigma(\tau_1^e)\times c_\sigma^\dagger(\tau_1^s)\ldots c_\sigma(\tau_k^e)c_\sigma^\dagger(\tau_k^s)\rangle\prod_\sigma\frac{1}{k_\sigma!}\times\text{Det}\begin{pmatrix}\Delta_\sigma(\tau_1^e,\tau_1^s) & \cdots & \Delta_\sigma(\tau_1^e,\tau_{k_\sigma}^s)\\ \cdots & \ddots & \cdots\\ \Delta_\sigma(\tau_{k_\sigma}^e,\tau_1^s) & \cdots & \Delta_\sigma(\tau_{k_\sigma}^e,\tau_{k_\sigma}^s)\end{pmatrix}. \quad (16)$$

The action is evaluated by Monte Carlo random walk in the space of expansion order k. The corresponding hybridization matrix changes in each accepted Monte Carlo update step. One-particle Green's function is measured as $G(\tau_j^e-\tau_i^s)=M_{i,j}$, where M is the inverse matrix of the hybridization function which can be obtained by the fast-update algorithm.[20]

In the mean time a direct measurement of the Matsubara frequency Green's function is allowed

$$G(i\nu_n) = \frac{1}{\beta}\sum_{i,j} e^{-i\nu_n \tau_i^s} M_{i,j} e^{i\nu_n \tau_j^e}. \quad (17)$$

Compared to the imaginary time measurement, it seems additional computational time is needed in order to sum up every matrix elements $M_{i,j}$. Haule[23] proposed to implement such measurement in every fast update procedure which only requires linear amount of time. In the weak-coupling CT-QMC we measured the Green's function at each accepted update step which greatly reduces the computational time. The weak-coupling CT-QMC normally yields a higher perturbation order k than the strong-coupling CT-QMC.[24] With respect to the convergence speed, the weak-coupling CT-QMC is comparable to the strong-coupling method under the above implementation together with a proper choice of α, since in strong-coupling CT-QMC more Monte Carlo steps are usually required in order to smooth the noise of the Green's function at imaginary time around $\beta/2$ or at larger Matsubara frequency points. Furthermore, the weak-coupling CT-QMC is much easier implemented for large cluster DMFT calculation, in which case the strong-coupling method needs to handle a big eigenspace. In this paper we mainly use the weak-coupling CT-QMC as impurity solver, while all the results can be obtained equally in the strong-coupling CT-QMC which was used as an accuracy check.

Similarly, we adapt Haule's implementation to calculate the two-particle Green's function in frequency space. In the weak-coupling CT-QMC, the noninteracting action has Gaussian form which ensures the applicability of Wick's theorem for measuring the two-particle Green's function

$$\chi_{\sigma\sigma'}(\nu_1,\nu_2,\nu_3,\nu_4) = T[\overline{G_\sigma(\nu_1,\nu_2)G_{\sigma'}(\nu_3,\nu_4)} - \delta_{\sigma\sigma'}\overline{G_\sigma(\nu_1,\nu_4)G_\sigma(\nu_3,\nu_2)}]. \quad (18)$$

The overline indicates the Monte Carlo average. In each Monte Carlo measurement step, $G(\nu,\nu')$ depends on two different arguments ν and ν', only in the average level $\overline{G(\nu,\nu')} = G(\nu)\delta_{\nu,\nu'}$ is a function of single frequency. In each fast-update procedure, the new and old $G(\nu,\nu')$ have a close relation which allows us to determine the updated Green's function $G^{\text{new}}(\nu,\nu')$ from the old one $G^{\text{old}}(\nu,\nu')$. Let us take adding pair of kink as example. Suppose before updating the perturbation order is k, then it is $k+1$ for the new M matrix. The new inserted pair is at $k+1$ row and $k+1$ column. The new and old two-frequency dependent Green's functions relate with each other in the following way:

$$G^{\text{new}}(\nu,\nu') - G^{\text{old}}(\nu,\nu') = \frac{M^{\text{new}}_{k+1,k+1}}{\beta} G^0(\nu)\{XL\cdot XR - XR\cdot e^{-i\nu\tau^s_{k+1}} - XL\cdot e^{i\nu'\tau^e_{k+1}} + e^{-i\nu\tau^s_{k+1}+i\nu'\tau^e_{k+1}}\}G^0(\nu'). \quad (19)$$

Here, $XL=\Sigma_{i=1}^{k} e^{-i\nu\tau_i^s} L_i$, $XR=\Sigma_{j=1}^{k} e^{i\nu'\tau_j^e} R_j$, and L_i, R_j have the same definition as in Ref 20. In every MC step, one only needs to calculate the Green's function when the update is accepted and only a few calculations are needed. A similar procedure for removing pairs, shifting end-point operation can be used. Such method is also applicable in the segment representation of the strong-coupling CT-QMC. In the weak-coupling CT-QMC, such an implementation greatly improves the calculating speed in the low-temperature and strong-interaction regime.[25]

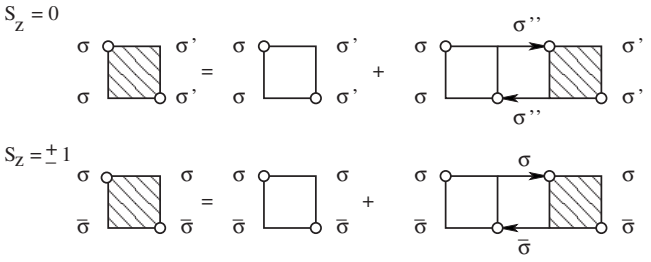

FIG. 2. $S_z=0$ (ph0) and $S_z=\pm 1$ (ph1) particle-hole channels of the DF vertex; between vertices there are two full DF Green's functions. The $S_z=\pm 1$ component is the triplet channel, while that for $S_z=0$ can be either singlet or triplet.

Once one obtains the two-frequency dependent Green's function in every Monte Carlo step, the two-particle Green's function can be determined easily from Eq. (18). The two-particle vertex is then given from the following equation:

$$\gamma_\omega^{\sigma\sigma'}(\nu,\nu') = \frac{\beta^2[\chi_\omega^{\sigma\sigma'}(\nu,\nu') - \chi_\omega^0(\nu,\nu')]}{g_\sigma(\nu)g_\sigma(\nu+\omega)g_{\sigma'}(\nu'+\omega)g_{\sigma'}(\nu')}, \quad (20)$$

where

$$\chi_\omega^0(\nu,\nu') = T[\delta_{\omega,0}g_\sigma(\nu)g_{\sigma'}(\nu') - \delta_{\sigma\sigma'}\delta_{\nu,\nu'}g_\sigma(\nu)g_\sigma(\nu+\omega)] \quad (21)$$

is the bare susceptibility. The multiparticle Green's function can also be constructed from the two-frequency dependent Green's function $G(\nu,\nu')$, but more terms appear from the Wick's theorem. Simply, by setting $\nu=\nu'$ the one-particle Green's function is obtained.

IV. MOMENTUM DEPENDENCE OF VERTEX

As mentioned earlier diagram (a) in Fig. 1 only gives the local contribution. The first nonlocal correction in the DF method is from diagram (b). Momentum dependence comes into this theory through the bubblelike diagram between the two vertices. The natural way to renormalize vertex is through the Bethe-Salpeter equation. Since the DMFT vertex is only a function of Matsubara frequency, the integral over internal momentum ensures that the full vertex only depends on the center of mass momentum q or $k'-k$. The Bethe-Salpeter equations in the particle-hole channel[18,19] are shown in Fig. 2.

From the construction of the DF method, we know the interaction of the DF comes from the two-particle vertex of the lattice fermion which is obtained through the DMFT calculation. In the Bethe-Salpeter equation, it plays the role as building block. The corresponding Bethe-Salpeter equations for these two channels are

$$\Gamma_q^{\mathrm{ph0},\sigma\sigma'}(k,k') = \gamma_q^{\sigma\sigma'}(k,k') - \frac{T}{N}\sum_{k''\sigma''} \gamma_q^{\sigma\sigma''}(k,k'') \times G^d(k'')G^d(k''+q)\Gamma_q^{\mathrm{ph0},\sigma''\sigma'}(k'',k'), \tag{22a}$$

$$\Gamma_{k'-k}^{\mathrm{ph1},\sigma\bar{\sigma}}(k,k+q) = \gamma_{k'-k}^{\sigma\bar{\sigma}}(k,k+q) - \frac{T}{N}\sum_{q'} \gamma_{k'-k}^{\sigma\bar{\sigma}}(k,k+q') \times G^d(k+q')G^d(k'+q') \times \Gamma_{k'-k}^{\mathrm{ph1},\sigma\bar{\sigma}}(k+q',k+q). \tag{22b}$$

Here, the short hand notation of spin configuration is used. $\gamma^{\sigma\sigma'}$ represents $\gamma^{\sigma\sigma\sigma'\sigma'}$, while $\gamma^{\sigma\bar{\sigma}\bar{\sigma}\sigma}$ is denoted by $\gamma^{\sigma\bar{\sigma}}$, where $\bar{\sigma}=-\sigma$. $\Gamma^{\mathrm{ph0(ph1)}}$ are the full vertices in the $S_z=0$ and $S_z=\pm 1$ channels, respectively. G^d is the full DF Green's function obtained from Sec. II which is kept unchanged in solving the Bethe-Salpeter equation. We solve the above equations directly in momentum space with the advantage that in this way we can calculate the susceptibility for any specific center of mass momentum q and it is convenient to use FFT for investigating larger lattice. In the above Bethe-Salpeter equations, we used the general form of the vertex function γ which depends on both frequency and momentum. But in the DF method, γ is only a function of frequency which means $\gamma_q^{\sigma\sigma'}(k,k')=\gamma_\omega^{\sigma\sigma'}(\nu,\nu')$. This leads to the fact that the full vertex calculated through the Bethe-Salpeter equation is a function of single transfer momentum. The center of mass momentum in the $S_z=0$ and $S_z=\pm 1$ channels are q and $k'-k$, respectively.

In Eq. (22) one has to sum up the internal spin indices in the $S_z=0$ channel which is not present in $S_z=\pm 1$ channel. One can decouple the $S_z=0$ channel into the charge and spin components $\gamma_{c(s)}=\gamma^{\sigma\sigma}\pm\gamma^{\sigma\bar{\sigma}}$ which can be solved separately, and the spin channel vertex function is exactly same as the vertex in $S_z=\pm 1$ channel (see, e.g., Ref. 19). This relation is true for the DMFT vertex and was also verified for the momentum dependent vertex in the DF method.[26]

Once the converged momentum dependent DF vertex is obtained, one can determine the corresponding DF susceptibility in the standard way by attaching four Green's functions to the DF vertex

$$\chi_d^{\sigma\sigma'}(q) = \chi_d^0(q) + \frac{T^2}{N^2}\sum_{k,k'} G_\sigma^d(k)G_\sigma^d(k+q) \times \Gamma^{\sigma\sigma'}(q)G_{\sigma'}^d(k')G_{\sigma'}^d(k'+q). \tag{23}$$

The momentum sum over $\mathbf{k}$ and $\mathbf{k}'$ can be performed independently by FFT, since the DF vertex $\Gamma^{\sigma\sigma'}(q)$ only depends on the center of mass momentum q.

Now the z-component DF spin susceptibility $\langle S^z\cdot S^z\rangle = 2(\chi_d^{\uparrow\uparrow}-\chi_d^{\uparrow\downarrow})$ can be determined from the spin channel component calculated above. In Fig. 3, $\tilde{\chi}^{zz}=\chi^{zz}-\chi_0^{zz}$ is shown for $U/t=4$ at temperatures $\beta t=4.0$ (left panel) and $\beta t=1.0$ (right panel). The momentum $\mathbf{q}_x$ and $\mathbf{q}_y$ run from 0 to 2π. The susceptibility strongly peaks at wave vector (π,π) and the peak value becomes larger with the lowering of temperature. The magnetic instability of the DF system is indicated by the enhancement of the DF susceptibility at (π,π). The effect of momentum dependence in vertex is clearly visible in this diagram. The bare vertex which is only a function of frequency becomes momentum dependent through the Bethe-Salpeter equation. Later on we will see that such momentum dependent vertex plays a very important role in the calculation of the lattice fermion susceptibility. Note in this diagram only the nontrivial DF spin susceptibility $\tilde{\chi}$ is shown, where the minimum locates at $(\pi,0)$ and $(0,\pi)$. The minimum of the full DF susceptibility χ still locates at $q=(0,0)$.

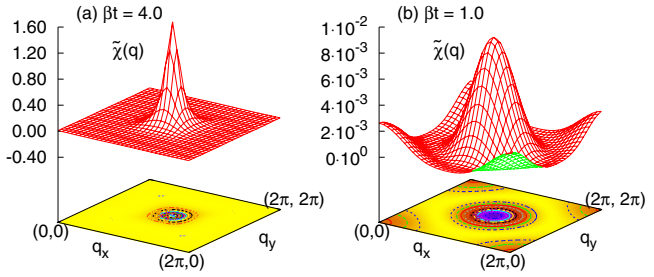

FIG. 3. (Color online) The nontrivial part of the DF spin susceptibilities as a function of momentum in 2D Hubbard model for $U/t=4.0$, $\beta t=1.0$ (right panel), and $\beta t=4.0$ (left panel). Here 32×32 momentum points are used in the first Brillouin zone.

V. LATTICE SUSCEPTIBILITY IN THE DF METHOD

The strong antiferromagnetic fluctuation in two-dimensional (2D) system is indicated by the enhancement of the DF susceptibility at the wave vector (π,π) shown in Fig. 3. This is the consequence of the deep relation between the Green's function of the lattice and the DF [see Eq. (4)]. In order to observe the magnetic instability of the lattice fermion directly, we calculated the lattice susceptibility based on the DF method. By differentiating the partition function in Eqs. (2) and (3) twice over the kinetic term, we obtain an exact relation between the susceptibility of the DF and lattice fermions. After some simplifications,[26] it is given by

$$\chi_f^{\sigma\sigma'}(q) = \chi_f^0(q) + \frac{T^2}{N^2}\sum_{k,k'} G'_\sigma(k)G'_\sigma(k+q)\Gamma^{\sigma\sigma'}(q)G'_{\sigma'}(k')G'_{\sigma'}(k'+q). \tag{24}$$

Here G' cannot be interpreted as a particle propagator. It is defined as

$$G'_\sigma(k) = \frac{G_\sigma^d(k)}{g_\nu[\Delta_\nu-\epsilon(k)]}. \tag{25}$$

Again, the sum is performed over internal momentum and frequency k,k' which is performed by FFT and rough summing up a few Matsubara points. As in Eq. (4), this equation established a connection between the lattice susceptibility and the DF susceptibility. From this point of view, it is easy to understand that the instability in the DF will lead to the instability in the lattice fermions.

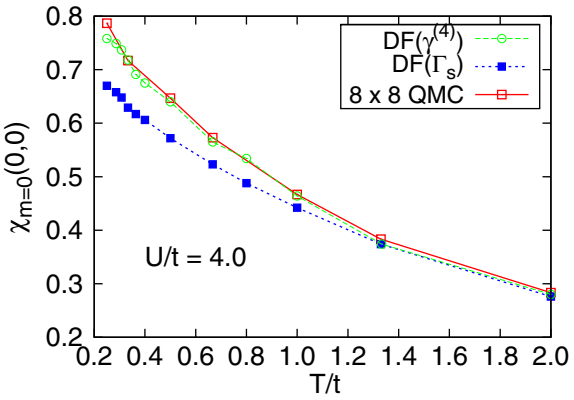

FIG. 4. (Color online) The uniform spin susceptibility of the DF calculated from the bare vertex (only frequency dependent) and the full vertex (vertex from the Bethe-Salpeter equation) for half-filled 2D Hubbard model at $U/t=4.0$ and various temperatures. These results basically reproduce the finite-size QMC solution.

One can also find relations for the multiparticle Green's function between the DF and the lattice fermions in the same way. This emphasizes the similar nature of the DF and lattice fermions except that DF possesses only nonlocal information, since the DMFT self-consistency ensures that the local DF Green's function is exactly zero.

In this paper, we used two different ways to calculate the lattice susceptibility $\chi_m(q)=2(\chi_f^{\uparrow\uparrow}-\chi_f^{\uparrow\downarrow})$. First we used the bare vertex $\gamma_\omega^{(4)}(\nu,\nu')$ which is obtained from the DMFT calculation. In contrast, the second calculation was performed using the full DF vertex in the spin channel $\Gamma_{s,q}(\nu,\nu')$. In both calculations, the full one-particle DF Green's function was used. The momentum dependent DF vertex is obtained through the calculation of the Bethe-Salpeter equation. By comparing these two calculations, we can understand the effect of the momentum dependence of the DF vertex. The solution of the lattice susceptibility is expected to be improved by using the momentum dependent DF vertex.

In Fig. 4 we plotted the results for the uniform susceptibility $\chi_{m=0}(0,0)$ by using both the bare and the full DF vertices. The lattice QMC result[27] is shown for comparison. The calculation is performed at $U/t=4.0$. The momentum sum is approximated over 32×32 points here. Both of these calculations reproduce the well-known Curie-Weiss law behavior. Surprisingly enough, by using the bare vertex we obtained the results which coincide with the QMC results better. We attribute it to the finite-size effect of QMC.[27] Moreo[27] showed that χ becomes smaller with the increase in the cluster size N. The 4×4 cluster calculation result for the same parameter locates above the solutions from 8×8 cluster calculation. Hence the results obtained from the full vertex calculation are expected to be more reasonable.

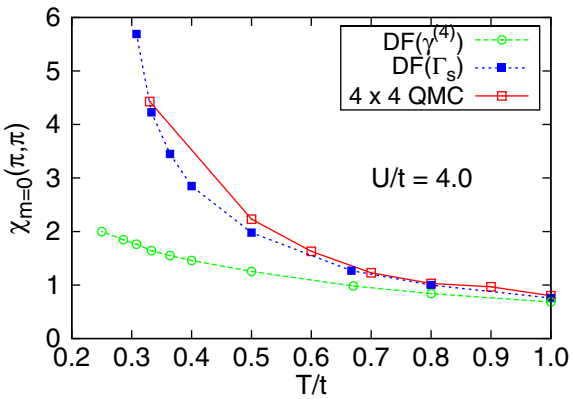

FIG. 5. (Color online) Uniform spin susceptibility at wave vector (π,π). The QMC results are obtained from Ref. 2.

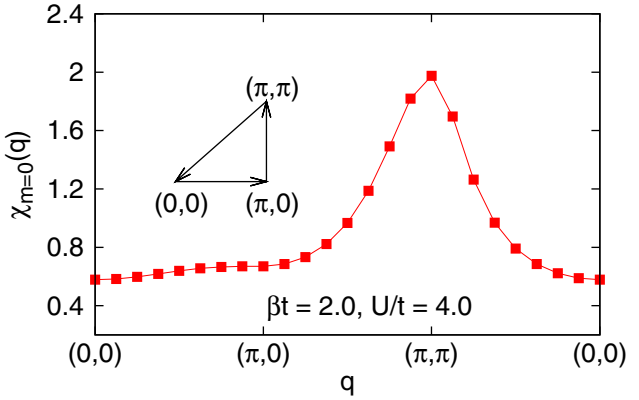

FIG. 6. (Color online) Momentum dependence of the spin susceptibility $\chi(q)$ at $\beta t=2.0$, $U/t=4.0$. The trajectory of q is shown in the inset.

The importance of the momentum dependence of the DF vertex is more clearly observed in the calculation of $\chi_m(\pi,\pi)$ shown in Fig. 5. Again, in this diagram QMC results[2] are shown for comparison. The same parameters are used as in Fig. 4. The results from the DF calculation with bare vertex do not reproduce the QMC solution. Even more serious, with the decrease in temperature the deviation becomes larger. In contrast, the calculation with the momentum dependent vertex gives a satisfactory solution. This shows the importance of the momentum dependence in the DF vertex function.

Figure 6 shows the momentum evolution of χ for fixed transfer frequency $\omega_m=0$. The path in momentum space is shown in the inset. From this diagram we can see that $\chi_m(\mathbf{q})$ reaches its maximum value at wave vector $\mathbf{q}=(\pi,\pi)$. Figure 7 shows the momentum evolution of the lattice susceptibility for $U/t=4.0$ and inverse temperatures $\beta t=1.0,4.0$. The in-

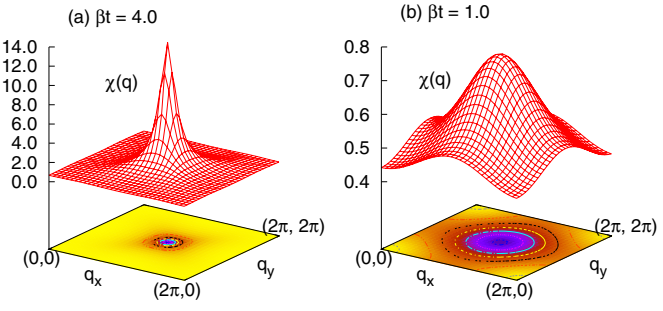

FIG. 7. (Color online) The lattice susceptibility for $U/t=4.0$ at two different temperatures $\beta t=4.0$ and $\beta t=1.0$ as a function of momentum calculated on 32×32 lattice.

creasing peak value at wave vector $\mathbf{q}=(\pi,\pi)$ indicates the formation of the antiferromagnetic order with the lowering of temperature. Compared to the nontrivial part of the DF susceptibility shown in Fig. 4, we can see that although the DF is not a real particle, it has similar nature as the lattice fermion. The magnetic instability appears in both the DF and the lattice fermion. The difference of the DF and the lattice fermion lies in the absence of local property in DF.

In summary, the comparison between the DF and QMC results shows the good performance of the DF method. Our calculation was carried out within 4 h for each value of temperature on average. In this sense, this method is cheap and reliable compared to the more computationally intensive lattice QMC calculation. Although we did self-consistent calculations in this paper (see Sec. II) under the current construction of the DF method, it is still possible to improve it. The full DF Green's function is calculated from the first two self-energy diagrams shown in Fig. 1 and kept unchanged in the calculation of the Bethe-Salpeter equations. This is not self-consistent indeed in the sense that the momentum dependent vertex (calculated from the Bethe-Salpeter equation) does not come into the calculation of the full DF Green's function. In the end the determination of the full vertex is not fully self-consistent. The better way is to consider the ladder approximation of the DF self-energy which can determine the DF Green's function and the full vertex on equal footing. It is called ladder dual fermion approximation (LDFA), in which the DF Green's function is determined from the full vertex and used to calculate the new full vertex in the next iteration. This loop is executed until the full DF Green's function and vertex do not change anymore. This approximation will improve the calculations for both the DF Green's function and the full vertex, especially for the one-dimensional (1D) Hubbard model where the single-site DMFT+DF calculation did not give the satisfied results.[28] More details and corresponding results will be presented elsewhere.

VI. LATTICE SUSCEPTIBILITY IN DΓA

Similar as the DF method, dynamical vertex approximation (DΓA) (Ref. 13) also bases on the two-particle local vertex. It deals with the lattice fermion directly without introducing any auxiliary field. The perturbative nature of this method ensures its validity at weak-coupling regime. Unlike in the DF method, DΓA takes the irreducible two-particle local vertex as building-block

$$\gamma^{-1}_{c(s)}(\nu,\nu';\omega)=\gamma^{-1}_{c(s),\mathrm{ir}}(\nu,\nu';\omega)-\chi_0(\nu;\omega)\delta_{\nu,\nu'}, \quad (26a)$$

$$\Gamma^{-1}_{c(s)}(\nu,\nu';q)=\gamma^{-1}_{c(s),\mathrm{ir}}(\nu,\nu';\omega)-\chi_0(\nu;q)\delta_{\nu,\nu'}. \quad (26b)$$

The spin and charge vertices are defined as $\gamma_{c(s)}=\gamma^{\uparrow\uparrow}\pm\gamma^{\uparrow\downarrow}$. Note that we used a different definition of the spin and charge channels which is opposite to that in reference.[13] We will follow the work of Toschi *et al.*[13] to determine the nonlocal self-energy function and then to calculate the lattice susceptibility.

The bare susceptibility is defined as

$$\chi_0(\nu;\omega)=-TG_{\mathrm{loc}}(\nu)G_{\mathrm{loc}}(\nu+\omega), \quad (27a)$$

$$\chi_0(\nu,q)=-\frac{T}{N}\sum_{\mathbf{k}}G^0(k)G^0(k+q), \quad (27b)$$

and the self-energy is calculated through the standard Schwinger-Dyson equation

$$\Sigma(k)=-U\frac{T^2}{N^2}\sum_{k',q}\Gamma_f(k,k';q)G^0(k')G^0(k'+q)G^0(k+q). \quad (28)$$

Here, the full vertex $\Gamma_f(k,k';q)$ is obtained by summing up all the channel dependent vertices and subtracting the double counted diagrams

$$\Gamma_f(k,k';q)=\frac{1}{2}\{[3\Gamma_c(\nu,\nu';q)-\Gamma_s(\nu,\nu';q)]-[\Gamma_c(\nu,\nu';\omega)-\Gamma_s(\nu,\nu';\omega)]\}, \quad (29)$$

which depends only on one momentum argument $\mathbf{q}$. The one-particle propagator is given by the DMFT lattice Green's function where the self-energy is purely local $G^0(k)=1/[i\nu-\epsilon(k)-\Sigma(\nu)]$. The lattice Green's function is then given from the Dyson equation $G^{-1}=G_0^{-1}-\Sigma$. The lattice spin susceptibility within the DΓA method is obtained by attaching four Green's functions on the vertex obtained in Eq. (26)

$$\chi(q)=\chi_0(q)+\sum_{\nu,\nu'}\chi_0(\nu,q)\Gamma_s(\nu,\nu';q)\chi_0(\nu',q). \quad (30)$$

To construct the bare susceptibility $\chi_0(q)$ and $\chi_0(\nu,q)$, we have two possible choices of the lattice Green's function. One is the DMFT lattice Green's function G^0. The other one is the Green's function G constructed by the nonlocal self-energy from the Dyson equation. In fact, the former is the way to determine the DMFT lattice susceptibility, which is not related with DΓA [Eq. (29)].

Before presenting the numerical results of the lattice susceptibility in DΓA, we take a deeper look at the analysis of Eq. (26)

$$\Gamma^{-1}_{c(s)}(\nu,\nu';q)=\gamma^{-1}_{c(s)}(\nu,\nu';\omega)-[\chi_0(\nu;q)-\chi_0(\nu;\omega)]\delta_{\nu,\nu'}. \quad (31)$$

The second term in the brackets on right hand side removes the local term from the bare susceptibility. The whole term in the brackets then represents only the nonlocal bare susceptibility. In order to compare to the DF method, we take the inverse form of Eq. (22)

$$\Gamma^{-1}_{d,cs}(\nu,\nu';q)=\gamma^{-1}_{c(s)}(\nu,\nu',\omega)+\frac{T}{N}\sum_{\mathbf{k}}G^d(k)G^d(k+q). \quad (32)$$

The above two equations are the same except for the last term. Since the local DF Green's function G^d_{loc} is zero, the bare DF susceptibility is purely nonlocal which coincides with the analysis of DΓA Bethe-Salpeter equation. There-

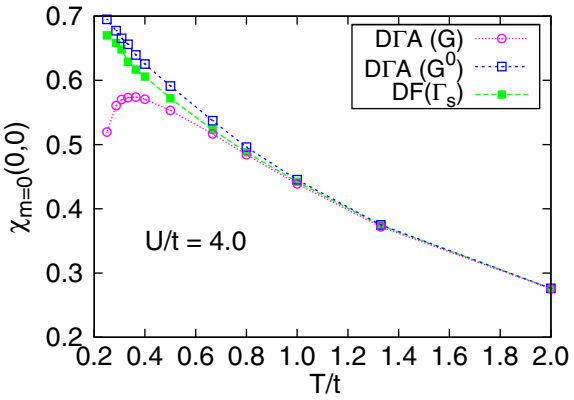

FIG. 8. (Color online) Comparison with the DΓA susceptibilities $\chi(0,0)$ which were obtained from both the DMFT lattice Green's function [DΓA (G^0)] and the full Green's function [DΓA (G)] (see context for more details).

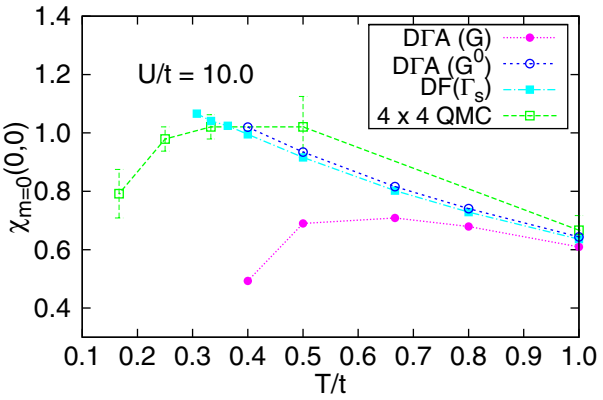

FIG. 9. (Color online) The comparison of the DF results and that of QMC for the uniform susceptibility at $U/t=10$. 4×4 QMC results (Ref. 27) also show the error bars.

fore, it will be not surprising if these two methods generate similar results. It is not easy to perform a term to term comparison between the DF method and DΓA although the bare susceptibilities have no local term in both of these methods. The one-particle Green's functions have different meanings in these two methods.

In Figs. 8 and 10, we presented the DΓA lattice susceptibility calculated from both the DMFT lattice Green's function [labeled as DΓA(G^0)] and the full Green's function [labeled as DΓA(G)]. The DF result from the calculation with the full DF vertex is replotted for comparison. In Fig. 8, the DΓA susceptibility calculated from the DMFT Green's function [DΓA(G^0)] is basically the same as the DF susceptibility only with some small deviations. The solutions for $T/t>1.0$ which are not shown here nicely repeat the DF and QMC results. The deviation between the DΓA and the DF method becomes smaller with the increase in temperature. The DΓA susceptibility calculated from the full Green's function [DΓA(G)] shows a different behavior at low-temperature regime which reaches its maximum value at $T/t\approx0.36$. The Hubbard model at strong-coupling regime can be mapped to the Heisenberg model; χ reaches a maximum at $T\approx J$, where J is the effective spin coupling constant given as $4t^2/U$. In order to investigate the behavior of $\chi(0,0)$ in the strong-coupling region, we further calculated the lattice susceptibility at $U/t=10.0$ which is shown in Fig. 9.

When the temperature is greater than 0.4, the DF method and DΓA [DΓA(G^0)] generate similar results compared to the QMC calculation. When the temperature is further decreased, the QMC susceptibility drops and peaks at 0.4 which coincides with the behavior of the Heisenberg model. The DF and the DΓA(G^0) susceptibility continuously grow up with the decrease in temperature. Although the DΓA with the full Green's function [DΓA(G)] shows a peak, it locates at $T/t=0.66$ which is larger than J. Moreover, DΓA(G) generates a large deviation from that of QMC. In this diagram, we only show the results for the DF approach at $T/t>0.3$ and for DΓA at $T/t>0.4$. The Bethe-Salpeter equation of the DF and DΓA methods has an eigenvalue approaching one when further lowering the temperature, which makes the access of lower temperature region hard. Figure 10 shows the results of DΓA susceptibilities at wave vector (π,π) for $U/t=4.0$ which is in the weak-coupling region. In contrast to the comparison for $\chi(0,0)$ results, the DΓA susceptibility calculated from the full Green's function DΓA (G) shows better agreement with the DF results. The deviation of DΓA(G^0) becomes larger at lower temperature regime.

The strange behavior of the DΓA lattice susceptibility calculated from the full Green's function [DΓA(G)] at $\mathbf{q}=(0,0)$ can be partially attributed to the non-self-consistency introduced in this method. The full vertex is calculated through the Bethe-Salpeter Eq. (26) by using the DMFT lattice Green's function G^0, while the four Green's functions attaching on this vertex are the full one. The better way is to determine the full vertex self-consistently from the corresponding full Green's function. Such non-self-consistent calculation might be one reason responsible for the unreasonable results at low-temperature region. The introduction of a Moriyaesque λ correction[29,30] to DΓA will further improve the performance of this method.

In both the DF method and the DΓA, the operation of inverting large matrices is required for solving the Bethe-Salpeter equation. Figure 11 shows the leading eigenvalue of Eqs. (22) and (26). As expected, the leading eigenvalue ap-

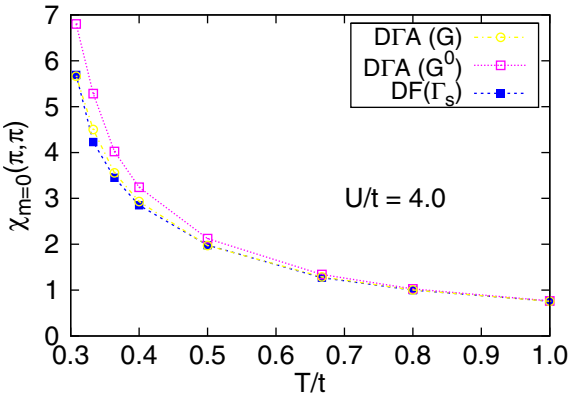

FIG. 10. (Color online) DΓA susceptibilities $\chi(\pi,\pi)$ at $U/t=4.0$. The susceptibility are determined from both of the DMFT and full lattice Green's function together with the vertex obtained from Eq. (29).

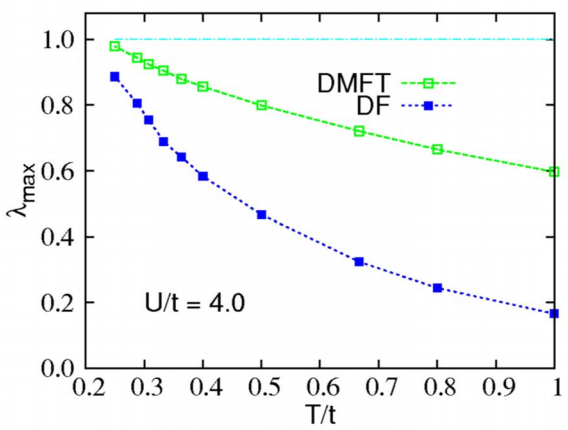

FIG. 11. (Color online) The evolution of maximum eigenvalue in spin channel against temperature for the DF method and the DΓA.

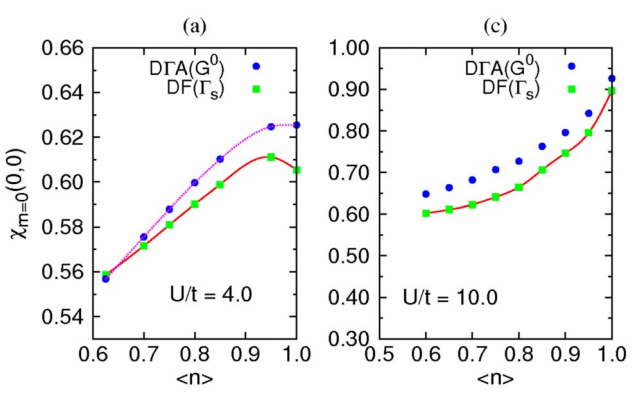

FIG. 12. (Color online) Uniform magnetic susceptibility is plotted as a function of doping at $\beta t=2.5$ and $U/t=4.0, 10.0$.

proaches one with decreasing temperature which directly indicates the magnetic instability of 2D system. The eigenvalues corresponding to the DF method always lie below of that from DΓA indicating the better convergence of the DF method. When the leading eigenvalues are close to 1, the matrix inversion in Eqs. (22) and (26) are ill defined, which prevents the investigation at very low temperature. The smaller values of the DF leading eigenvalue also indicate the effectively weak-coupling nature of the DF which will be discussed more detailed elsewhere.

We also calculated the uniform susceptibility at away half-filling. In the strong-coupling limit, the Hubbard model is equivalent to the Heisenberg model with coupling constant $J=4t^2/U$. The consequence of doping is to effectively decrease the coupling J, which yields the increasing behavior of χ with doping. The finite-size QMC calculation[27,31] observed a slightly increasing χ with very small doping at strong interaction or in the low-temperature region. Here, we did a similar calculation at $\beta t=2.5$ and $U/t=4, 10$. Since the DF method and the DΓA do not suffer from the finite-size problem, we would expect to observe the similar behavior of the susceptibility in these two methods. In DΓA the susceptibility was calculated from the DMFT Green's function G^0 and the vertex obtained from Eq. (29). As shown in Fig. 12 at $U/t=4.0$ the susceptibility χ slightly increases in the weak doping region where δ is around 0.05. DF results clearly show such behavior; DΓA(G^0) also gave a signal of it. Further doping the system, both the DΓA(G^0) and the DF susceptibility decrease which coincides with the QMC calculation. With the increase in the interaction, we would expect to see the enhancement of this effect. However our calculation indicates that such increasing-decreasing behavior disappears at strong-coupling and low-temperature regimes. Both the DΓA and the DF methods give the same decreasing curve which contradict to QMC result.[27] The results will most likely be further improved by including the higher order vertex or performing the cluster DMFT+DF/DΓA calculations.[28]

VII. CONCLUSION

In this paper, we extended both the DF and DΓA methods to calculate the lattice susceptibility. The full vertices of the dual and the lattice fermions are calculated through the Bethe-Salpeter equations in the particle-hole channels. The magnetic instability appeared in both the DF and real fermions. The lattice spin susceptibility calculated from both methods gave satisfied results compared to QMC calculation at $U/t=4.0$. The DF method generated large corrections to DMFT for the lattice susceptibility at wave vector $\mathbf{q}=(\pi,\pi)$. The DΓA did not generate equally good results for the lattice susceptibility at $\mathbf{q}=(0,0)$ and (π,π). Although they are supposed to be weak-coupling methods, at $U/t=10.0$ these two methods generated reliable results at high-temperature region, while both of them failed to reproduce the Heisenberg physics. We expect this will be cured by LDFA and the cluster DMFT+DF/DΓA calculations. The DF method always generates smaller eigenvalues indicating the better convergence. The implementation of DF method in momentum space greatly improves the calculational speed and makes it easier to deal with larger size lattice.

ACKNOWLEDGMENTS

We would like to thank the condensed matter group of A. Lichtenstein at Hamburg University for their hospitality in particular for the discussions and open exchange of data with H. Hafermann. G.L. and H.L. would like to thank Philipp Werner for his help in implementing the strong-coupling CT-QMC code.

[1] N. E. Bickers, D. J. Scalapino, and S. R. White, Phys. Rev. Lett. **62**, 961 (1989).
[2] N. E. Bickers and S. R. White, Phys. Rev. B **43**, 8044 (1991).
[3] Y. M. Vilk and A.-M. S. Tremblay, J. Phys. Chem. Solids **56**, 1769 (1995).
[4] Y. M. Vilk, L. Chen, and A. M. S. Tremblay, Phys. Rev. B **49**, 13267 (1994).
[5] W. Metzner and D. Vollhardt, Phys. Rev. Lett. **62**, 324 (1989).
[6] E. Müller-Hartmann, Z. Phys. B: Condens. Matter **57**, 281 (1984).
[7] A. Georges, G. Kotliar, W. Krauth, and M. J. Rozenberg, Rev. Mod. Phys. **68**, 13 (1996).
[8] M. H. Hettler, A. N. Tahvildar-Zadeh, M. Jarrell, T. Pruschke, and H. R. Krishnamurthy, Phys. Rev. B **58**, R7475 (1998).
[9] G. Kotliar, S. Y. Savrasov, G. Palsson, and G. Biroli, Phys. Rev. Lett. **87**, 186401 (2001).
[10] S. Okamoto, A. J. Millis, H. Monien, and A. Fuhrmann, Phys. Rev. B **68**, 195121 (2003).
[11] M. Potthoff, Eur. Phys. J. B **36**, 335 (2003).
[12] T. Maier, M. Jarrell, T. Pruschke, and M. H. Hettler, Rev. Mod. Phys. **77**, 1027 (2005).
[13] A. Toschi, A. A. Katanin, and K. Held, Phys. Rev. B **75**, 045118 (2007).
[14] A. N. Rubtsov, M. I. Katsnelson, and A. I. Lichtenstein, Phys. Rev. B **77**, 033101 (2008).
[15] H. Kusunose, J. Phys. Soc. Jpn. **75**, 054713 (2006).
[16] V. I. Tokar and R. Monnier, arXiv:cond-mat/0702011 (unpublished).
[17] C. Slezak, M. Jarrell, T. Maier, and J. Deisz, arXiv:cond-mat/0603421 (unpublished).
[18] A. Abrikosov, L. Gorkov, and I. Dzyaloshinski, *Methods of Quantum Field Theory in Statistical Physics* (Dover, New York, 1963).
[19] P. Nozieres, *Theory of Interacting Fermi Systems* (Benjamin, New York, 1964).
[20] A. N. Rubtsov, V. V. Savkin, and A. I. Lichtenstein, Phys. Rev. B **72**, 035122 (2005).
[21] P. Werner, A. Comanac, L. deMedici, M. Troyer, and A. J. Millis, Phys. Rev. Lett. **97**, 076405 (2006).
[22] P. Werner and A. J. Millis, Phys. Rev. B **74**, 155107 (2006).
[23] K. Haule, Phys. Rev. B **75**, 155113 (2007).
[24] E. Gull, P. Werner, A. Millis, and M. Troyer, Phys. Rev. B **76**, 235123 (2007).
[25] In fact, the improvement is more obvious for larger M matrices. The strong-coupling CT-QMC and the weak-coupling CT-QMC require approximately the same amount of CPU time although in the weak-coupling case the average perturbation order is higher than in the strong-coupling case.
[26] S. Brener, H. Hafermann, A. N. Rubtsov, M. I. Katsnelson, and A. I. Lichtenstein, Phys. Rev. B **77**, 195105 (2008).
[27] A. Moreo, Phys. Rev. B **48**, 3380 (1993).
[28] H. Hafermann, S. Brener, A. N. Rubtsov, M. I. Katsnelson, and A. I. Lichtenstein, Pis'ma Zh. Eksp. Teor. Fiz. **86**, 769 (2007).
[29] K. Held, A. A. Katanin, and A. Toschi, arXiv:0807.1860 (unpublished).
[30] A. A. Katanin, A. Toschi, and K. Held, arXiv:0808.0689 (unpublished).
[31] L. Chen and A.-M. S. Tremblay, Phys. Rev. B **49**, 4338 (1994).